Application of Geometrically Nonlinear Metamaterial Device for Structural Vibration Mitigation

Author(s):
Chondrogiannis, Kyriakos Alexandros; Dertimanis, Vasilis; Chatzi, Eleni

Publication date:
2022

Permanent link:
https://doi.org/10.3929/ethz-b-000574194

Originally published in:
Conference Proceedings of the Society for Experimental Mechanics Series 1, https://doi.org/10.1007/978-3-031-04086-3_17

Funding acknowledgement:
813424 - INNOVATIVE GROUND INTERFACE CONCEPTS FOR STRUCTURE PROTECTION (EC)

Application of Geometrically Nonlinear Metamaterial Device for Structural Vibration Mitigation

Kyriakos Alexandros Chondrogiannis[1], Vasilis Dertimanis[1] and Eleni Chatzi[1]

[1] Department of Civil, Environmental and Geomatic Engineering

ETH Zürich

Stefano-Franscini-Platz 5, 8093 Zurich, Switzerland

e-mail: {Chondrogiannis, v.derti, chatzi}@ibk.baug.ethz.ch

ABSTRACT

One of major challenges encountered by civil structures throughout their life cycle pertains to exposure to dynamic loadings; with earthquakes representing an extreme case of such a load. The frequency content of a dynamic excitation is of primary importance not only because of the potential resonance it induces, but also due to limitations that arise for the capabilities of vibration mitigation devices. A recently emerging technology for civil structure applications includes the development of metamaterial configurations. These are structures, which are formed by periodic arrangement of a fundamental component design, termed the unit-cell. They can offer impressive filtering properties within specific frequency ranges; the so-called band-gaps. Considering the low frequency content of earthquake excitation, a design that features a band-gap in the lower frequency range is required. In this study, the potential of a geometrically nonlinear design for vibration mitigation purposes is investigated for lowering of the corresponding band-gap. The system consists in the periodic arrangement of nonlinear unit cells, each including a triangular arch configuration, which under large displacement considerations can produce not only geometrically nonlinear behavior, but also negative stiffness effects. Analytical derivations result to the determination of the amplitude depended band-gap of the system. The proposed configuration is attached to a target structure subjected to protection. An assessment on the capabilities of the device towards this direction was performed via numerical analyses, revealing considerable effectiveness. Acceleration response, as well as energy related measures are considered in the evaluation of the system's performance. An additional potential, which the proposed configuration can offer, refers to the applicability of the system for retrofitting purposes of existing structures. It is concluded that the system can offer significant vibration mitigation capabilities, while further study and development of the design, taking into consideration constructability limitations, can lead to an efficient passive vibration absorption device.

Keywords: metamaterials, vibration mitigation, geometric nonlinearities, structural protection, negative stiffness

INTRODUCTION

Vibration mitigation devices target the counteraction of the effects of adverse dynamic loading, with particular focus on earthquake excitation. A broadly exploited solution in this direction is that of the tuned mass damper [1]. A linear attachment to a primary system leads to significant vibration attenuation capabilities at specific frequencies, which under proper adjustment can be tuned to match the natural frequency of the protected structure. Extension of this concept, leads to the study of nonlinear attachments, investigating nonlinear targeted energy transfer phenomena [2].

Recent developments in vibration absorption devices study the effect of metamaterial configurations [3]–[5]. These are formations of repeating patterns of a fundamental design, which is called the unit cell. They can lead to extraordinary filtering properties within a specified frequency range, called the band-gap [6], [7]. These stop-bands can be created by Bragg scattering phenomena, related to the periodicity of the lattice, or by local resonance effects, utilizing similar principles to the tuned mass damper [8], [9]. Several studies investigate the application of linear metamaterial designs for structural protection. Realistic

application studies include designs in the form of barriers, inserted between the soil and a protected structure, or foundations that support the weight of the structure [10], [11].

In an attempt to explore the full potential that metamaterial configurations can offer by widening the band-gap range, nonlinear behavior is investigated. Geometrically nonlinear behavior, negative stiffness elements, as well as non-smooth phenomena in the form of impacts are being studied in the literature as potential solutions for optimizing the designs [12]–[16]. In the works of Chen et al. [17], [18] and Al-Shudeifat et al. [19] negative stiffness elements are investigated in the form of shallow arch configurations for nonlinear composite structures and energy sink applications. The current study utilizes triangular arch designs that produce geometrically nonlinear behavior, in a metamaterial configuration for vibration mitigation purposes.

NONLINEAR UNIT CELL

In the current work, geometrically nonlinear behavior is considered for metamaterial development. This fundamental configuration consists of a rigid support of mass m, to which a triangular arch is attached, connected to mass μ, as depicted in Figure 1. It is formed by two identical linear springs of stiffness k_n in triangular arrangement. As the tip of the arch undergoes large displacements, geometrically nonlinear behavior occurs, which leads to negative stiffness phenomena. Successive cells are elastically interconnected with linear springs of stiffness k, while a dashpot element is considered both at the connection of adjacent cells and between the masses of each cell, with damping coefficients c and c_n respectively.

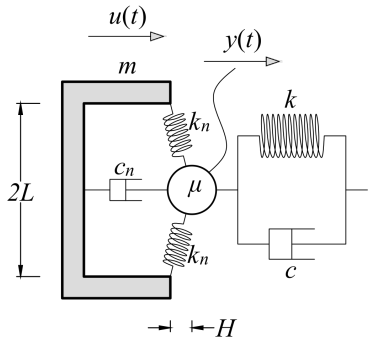

Figure 1: Schematic representation of the geometrically nonlinear unit cell.

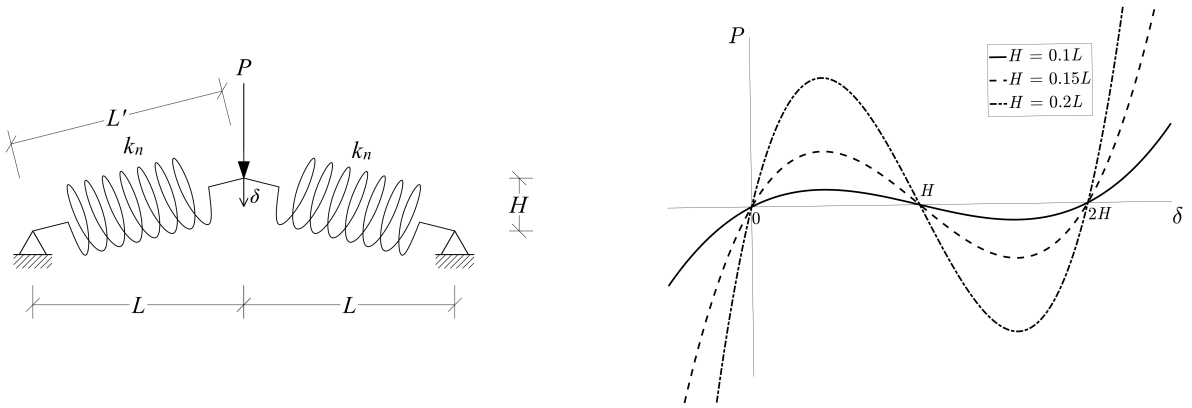

(a) (b)

Figure 2: (a)-Triangular arch configuration, (b)-Nonlinear equilibrium path.

GEOMETRICALLY NONLINEAR BEHAVIOR

By examining the nonlinear configuration of the system depicted in Figure 2, it is interesting to focus on the nonlinear equilibrium path that it is created. Although the behavior of the system is clearly nonlinear, as inferred from the equilibrium

path in Figure 2, elastic behavior is present throughout the deformation. A set of symmetric equilibrium points is identified for $\delta = 0$ and $\delta = 2H$, representing the two symmetric positions, where the springs are at their natural length. Additionally, a third equilibrium point can be pinpointed for $v(t) = H$, which is unstable and corresponds to the position where the two springs are aligned. It is observed that the system is able to not only produce nonlinear behavior but further exhibits negative stiffness phenomena, for specific displacement values, which is a result of its bi-stable nature. The higher the initial height value H the more intense the negative stiffness phenomena, as inferred from the slope of the nonlinear path in Figure 2. The exact nonlinear force-displacement relation can be calculated in Eqn. (1). This function of δ can be approximated with a 3rd order polynomial, after using Taylor series expansion about $v = H$, according to Eqn. (2) [19].

$$P(\delta) = 2 \cdot k_n \cdot L' \left(1 - \sqrt{\frac{\left(\frac{L}{H}\right)^2 + \left(1 - \frac{\delta}{H}\right)^2}{\left(\frac{L}{H}\right)^2 + 1}} \right) \frac{1 - \frac{\delta}{H}}{\sqrt{\left(\frac{L}{H}\right)^2 + \left(1 - \frac{\delta}{H}\right)^2}} \tag{1}$$

where $L' = \sqrt{L^2 + H^2}$

$$\begin{aligned} P(\delta) &\approx k_1 \cdot (\delta - H) + k_2 \cdot (\delta - H)^3, \\ k_1 &= -2 \cdot k_n \cdot \left(\frac{L'}{L} - 1 \right) \\ k_2 &= \frac{k_n L'}{L^3} \end{aligned} \tag{2}$$

DISPERSION RELATION

An important aspect that needs to be identified in a metamaterial design is the dispersion relation. This provides a useful indication with respect to the frequency ranges that are filtered by the configuration revealing the band-gap of the system. In order to identify this relation, it is crucial to consider an infinite lattice of identical unit cells, as shown in Figure 3. This consideration enables the assumption of periodic solutions for the oscillation of the cells [12], as in Eqn. (3).

$$\begin{aligned} u_{j\pm1}(t) &= \left(U_1 \mathrm{e}^{\mathrm{i}\omega t} + \bar{U}_1 \mathrm{e}^{-\mathrm{i}\omega t} \right) \mathrm{e}^{\pm \mathrm{i}q} \\ v_{j\pm1}(t) &= \left(V_1 \mathrm{e}^{\mathrm{i}\omega t} + \bar{V}_1 \mathrm{e}^{-\mathrm{i}\omega t} \right) \mathrm{e}^{\pm \mathrm{i}q} \\ v(t) &= u(t) - y(t) \end{aligned} \tag{3}$$

Where $u_j(t)$ and $y_j(t)$ are the displacements of mass m and μ of the j-th cell respectively, q is the reduced wave number, ω is the angular frequency and $\mathrm{i} = \sqrt{-1}$.

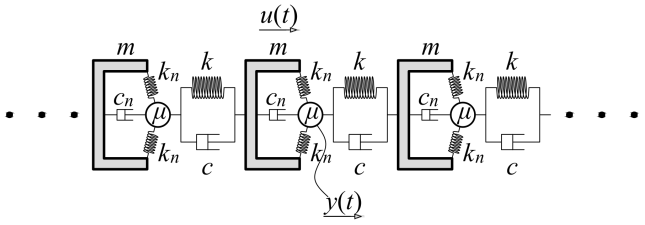

Figure 3: Schematic representation of the infinite lattice, required for the calculation of the analytical dispersion relation.

After the application of Eqn. (2) for the approximation of the nonlinear interaction between mass m and μ for each unit cell, the equations of motion of the system read:

$$
\begin{aligned}
&m\ddot{u}_j(t)+k[u_j(t)-(u_{j-1}(t)-v_{j-1}(t))]+k_1v_j(t)+k_2v_j(t)^3=0\\
&\mu(\ddot{u}_j(t)-\ddot{v}_j(t))+k(u_j(t)-v_j(t)-u_{j+1}(t))-k_1v_j(t)-k_2v_j(t)^3=0
\end{aligned}
\tag{4}
$$

Substitution of Eqn. (3) into Eqn. (4) yields the dispersion relation of the system as follows:

$$
\cos(q)=\frac{2k\left(k_1+3k_2V_1\bar{V}_1\right)-\left(m+\mu\right)\left(k+k_1+3k_2V_1\bar{V}_1\right)\omega^2+m\mu\omega^4}{2k\left(k_1+3k_2V_1\bar{V}_1\right)}
\tag{5}
$$

Focusing on the above relation, it is important to analyze its dependence on the relative oscillation amplitude between the nonlinearly connected masses of each cell. This is included in the ansatz of v in Eqn. (3) for V_1 and $\bar{V}_1$ coefficients and appears in Eqn. (5), in the form of $V_1\bar{V}_1$ ($V_1\bar{V}_1=|V_1|^2$). Solution of Eqn. (5) for discrete frequencies is possible after defining the value of $|V_1|$ and therefore $V_1\bar{V}_1$ parameter. Figure 4 depicts the solution of the dispersion relation of the infinite lattice. In contrast to linear systems, this is a 3-dimensional representation that contains the additional parameter of the oscillation amplitude. The acoustic and optical branches appear in the solution, which form the limits of the corresponding band-gap. It is observed that the band-gap shifts into the frequency domain depending on the oscillation amplitude, as well as changes in width. For lower amplitudes, the triangular arch oscillates at small angles, thus establishing the system more flexible and therefore lowers the band-gap in the frequency range. For higher oscillation amplitudes, where the triangular arch experiences larger angles, the system becomes stiffer with a result of increasing the opening frequency of the band-gap. Additionally, for these high oscillation amplitudes, the width of the band-gap is increased, as the optical branch shifts significantly to higher frequencies.

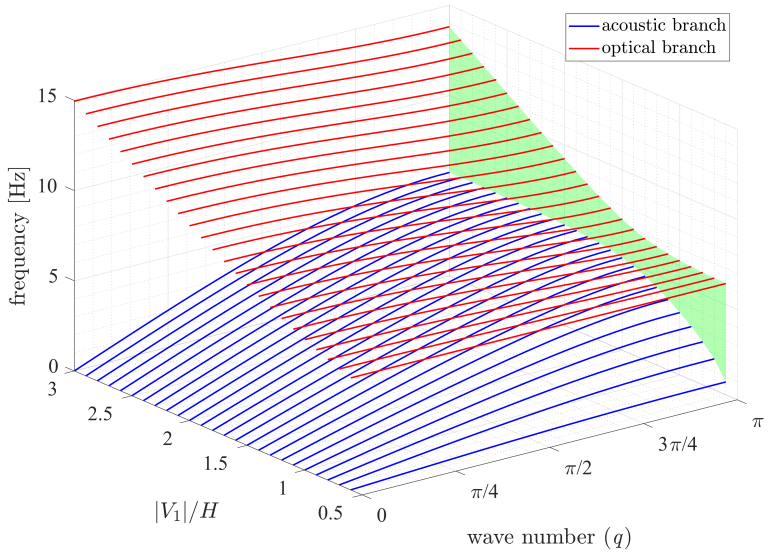

Figure 4: Dispersion curves of the infinite lattice. Evolution of the band-gap with respect to the oscillation amplitude is denoted with green color. (m=2, k=10^3, μ=1, k_n=$2\cdot10^3$, H=0.15, L=0.5).

NUMERICAL VALIDATION

For the validation of the dynamic properties of the nonlinear system, numerical analyses have been performed. For this purpose, a finite lattice of N identical unit cells has been considered, as shown in Figure 5.

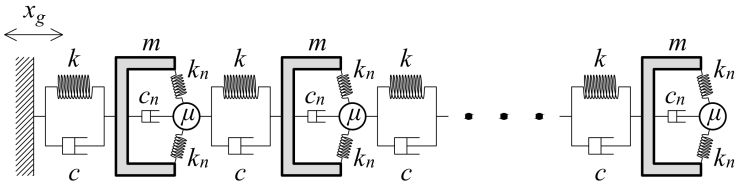

Figure 5: Schematic representation of a finite lattice, used for the numerical estimation of the dispersion relation.

The configuration of Figure 5 has been simulated numerically in MATLAB® environment, with the use of the *ode45* function (AbsTol=$1\cdot10^{-10}$, RelTol=$1\cdot10^{-7}$). For this purpose, the system is brought to a nonlinear state-space form:

$$\begin{aligned} &\dot{z}(t) = g(z(t), x_g(t)) \\ &z = \left[u_1, \dot{u}_1, y_1, \dot{y}_1 \mid \ \ldots \ \mid u_N, \dot{u}_N, y_N, \dot{y}_N\right]^T \end{aligned} \tag{6}$$

Where $u_j(t)$ and $y_j(t)$ are the displacements of mass m and μ respectively of the j-th unit cell.

The equations of motion of the 1st unit cell are formed as:

$$\begin{aligned} &m\ddot{u}_1 + c(\dot{u}_1 - \dot{x}_g) + c_n(\dot{u}_1 - \dot{y}_1) + k(u_1 - x_g) + F_{nl}^1 = 0 \\ &m\ddot{y}_1 + c(\dot{y}_1 - \dot{u}_2) + c_n(\dot{y}_1 - \dot{u}_1) + k(y_1 - u_2) - F_{nl}^1 = 0 \end{aligned} \tag{7}$$

For the i-th unit cell, the equations of motion are formed as:

$$\begin{aligned} &m\ddot{u}_i + c(\dot{u}_i - \dot{u}_{i-1}) + c_n(\dot{u}_i - \dot{y}_i) + k(u_i - u_{i-1}) + F_{nl}^i = 0 \\ &m\ddot{y}_i + c(\dot{y}_i - \dot{u}_{i+1}) + c_n(\dot{y}_i - \dot{u}_i) + k(y_i - u_{i+1}) - F_{nl}^i = 0 \end{aligned} \tag{8}$$

For the last (N-th) unit cell they are formed as:

$$\begin{aligned} &m\ddot{u}_N + c(\dot{u}_N - \dot{u}_{N-1}) + c_n(\dot{u}_N - \dot{y}_N) + k(u_N - u_{N-1}) + F_{nl}^N = 0 \\ &m\ddot{y}_N + c_n(\dot{y}_N - \dot{u}_N) - F_{nl}^N = 0 \end{aligned} \tag{9}$$

Where $F_{nl}^j = F_{nl}^j(x_{rel}^j) = P(x_{rel}^j)$, $x_{rel}^j = u_j - y_j$ and for $P(x_{rel}^j)$ the exact relation of Eqn. (1) is used.

For the analyses in this section, the following parameters are considered, while damping is not included ($c = 0$, $c_n = 0$):

$$m = 2, \ \ \mu = 1, \ \ k = 1\cdot10^3, \ \ k_n = 2\cdot10^3, \ \ L = 0.5, \ \ H = 0.15, \ \ N = 64$$

The configuration is excited by base excitation x_g, which follows a sine-sweep function in the frequency range 0.1-20.0 Hz for a time period of 50 seconds, as shown in Figure 6.

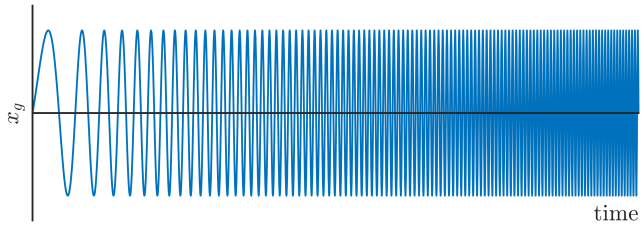

Figure 6: The employed input sine-sweep excitation in the frequency range 0.1-20.0 Hz.

In order to estimate the dispersion relation of the setup, a two dimensional Fast Fourier Transform in time and in space is applied to the output states [20]. In this set of analyses, the reference output state was considered to be the displacement of mass m of each unit cell. Figure 7 shows the numerical estimations of the dispersion curves in comparison to the analytical approach. The two methods result in good agreement for both the acoustic and the optical branch. Furthermore, the shifting of the dispersion curves, and the corresponding widening of the band-gap, in the frequency domain, depending on the oscillation amplitude is evident in both the analytical and numerical results.

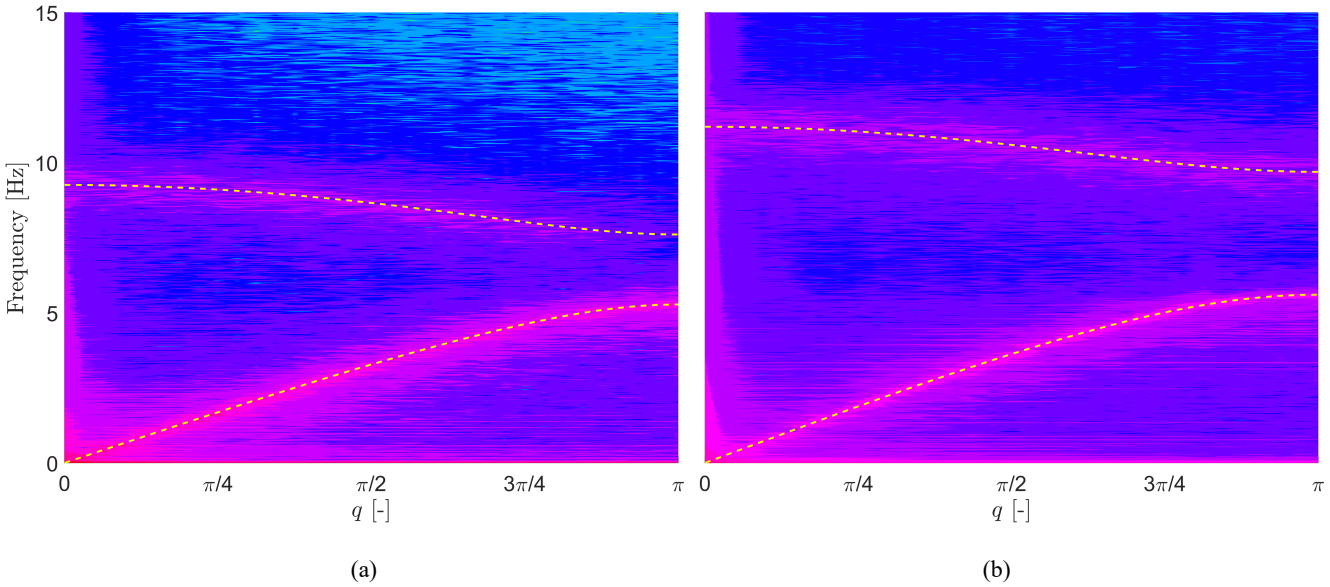

Figure 7: Comparison of the numerical against the analytically computed dispersion curves. The contour plot corresponds to the numerical analyses and dashed lines to the analytical solutions. (a)-$|V_1|=1.6H$, (b)-$|V_1|=2.1H$. (m=2, k=10^3, μ=1, k_n=$2\cdot10^3$, H=0.15, L=0.5).

APPLICATION OF THE METAMATERIAL DEVICE FOR VIBRATION MITIGATION

In this section, the effect of the metamaterial configuration is evaluated with respect to its vibration mitigation capabilities. For this purpose, the model of Figure 8 in studied. It consists of a reference structure founded on a raft foundation. The basement is laterally connected to the metamaterial configuration, while at the bottom the shear connection as a result of soil-structure interaction is considered. A simplification of this setup results in the model in Figure 9. The shear connection between the basement and the soil is replaced by an elastic connection in the horizontal direction, while its stiffness K_{SSI} is calculated following the work of Gazetas [21]. Vertically propagating shear waves are considered in this study. In that respect, in the simplified model, the excitation x_g is applied to both ends of the setup, acting in the horizontal direction, as shown in Figure 9.

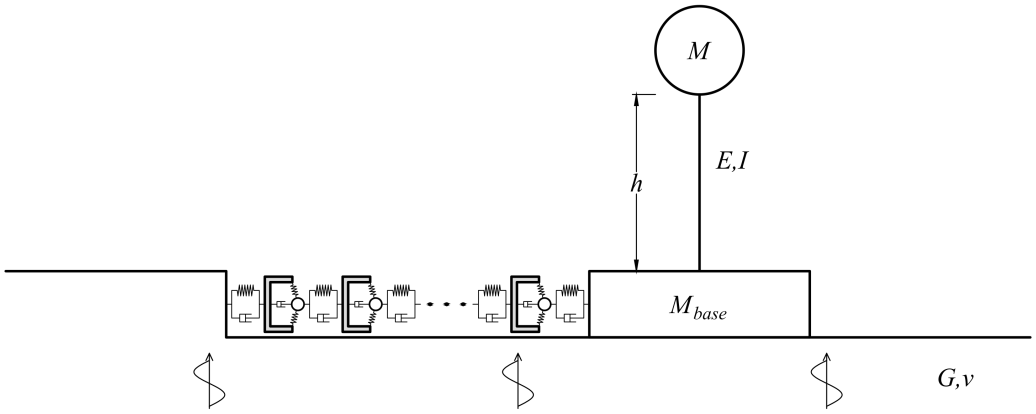

Figure 8: Structure to metamaterial coupling.

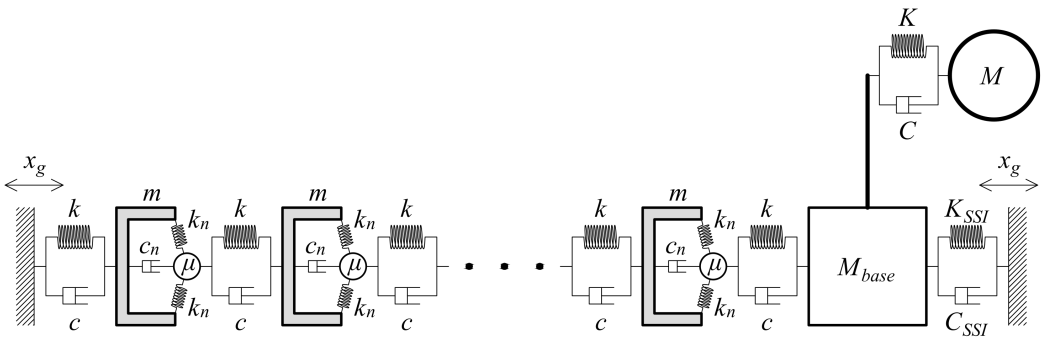

Figure 9: Simplified model considering soil-structure interaction, in the form of its stiffness and damping properties K_{SSI} and C_{SSI} respectively, acting in the horizontal direction.

The parameters of the metamaterial configuration that were used are the following:

$$m = 2.25 \ \text{Mgr}, \ \mu = 1.125 \ \text{Mgr}, \ k = 45 \cdot 10^6 \ \text{kN/m},$$
$$k_n = 3400 \ \text{kN/m}, \ c_n = 10 \ \text{Mgr/s}, \ L = 0.5 \ m, \ H = 0.05 \ m$$

While the damping ratio in the connection between the cells was set to 5%.

The protected structure corresponds to an equivalent of a 5-story building with the following parameters:

$$M = 50 \ \text{Mgr}, \ M_{base} = 24.4 \ \text{Mgr}, \ K = 6040 \ \text{kN/m}$$

While 5% damping is considered.

Finally, the stiffness properties of the soil-structure interaction is calculated, according to the work of Gazetas [21], as $K_{SSI} = 462349$ kN/m, with 5% damping. This calculation corresponds to soil properties $v_s = 150$ m/s, $\rho = 1700$ kg/m^3, $v = 0.5$, considering undrained conditions.

For the evaluation of the system's performance in terms of mitigation of vibrations, numerical analyses have been performed for the nonlinear configuration, according to the previous section. The equations of motion of the system need to be adjusted for the final (N-th) unit cell, compared to the previous section as:

$$\begin{aligned} &m\ddot{u}_N + c(\dot{u}_N - \dot{u}_{N-1}) + c_n(\dot{u}_N - \dot{y}_N) + k(u_N - u_{N-1}) + F_{nl}^N = 0 \\ &m\ddot{y}_N + c(\dot{y}_N - \dot{x}_{base}) + c_n(\dot{y}_N - \dot{u}_N) + k(y_N - x_{base}) - F_{nl}^N = 0 \end{aligned} \tag{10}$$

For the basement, the equations of motion are formed as:

$$\begin{aligned} &M_{base}\ddot{x}_{base} + c(\dot{x}_{base} - \dot{y}_N) + k(x_{base} - y_N) + C_{SSI}(\dot{x}_{base} - \dot{x}_g) + \\ &+K_{SSI}(x_{base} - x_g) + C(\dot{x}_{base} - \dot{X}) + K(x_{base} - X) = 0 \end{aligned} \tag{11}$$

Finally, for the top mass the equations of motion are formed as:

$$M\ddot{X} + C(\dot{X} - \dot{x}_{base}) + K(X - x_{base}) = 0 \tag{12}$$

where x_{base} and X are the displacements of the basement and top mass respectively.

The state-space vector of Eqn. (6) is updated in order to include the added degrees of freedom:

$$z = \left[u_1, \dot{u}_1, y_1, \dot{y}_1 \mid \ \ldots \ \mid u_N, \dot{u}_N, y_N, \dot{y}_N \mid x_{base}, \dot{x}_{base} \mid X, \dot{X} \right]^T \tag{13}$$

As a first step, harmonic base excitation is applied in the form of ground acceleration $\ddot{x}_g(t) = A\sin(\omega t)$, where a constant acceleration amplitude A is considered for all analyses. These were applied for 30 seconds, for discrete frequencies. The maximum response amplitude was recorded and plotted versus the corresponding excitation frequency, as shown in Figure 10. The results are further compared to the response of the unprotected structure, where soil-structure interaction is considered. It is observed that the nonlinear system is able to reduce the acceleration response at the top mass for a frequency range > 1 Hz, compared to the unprotected configuration. As the number of unit cells that are included in the metastructure is increased, the acceleration mitigation effect is more significant for frequencies >1 Hz. The inclusion of one unit cell results in slight reduction of the accelerations around the resonance frequency, with respect to the unprotected case. The inclusion of more cells in the lattice affects a wider range of frequencies, as observed in Figure 10. Interestingly, the reduction of acceleration amplitudes at resonance frequency is not improved for a 5-cell lattice compared to the 2-cell. The most prominent effects for the longer lattice are focused in frequencies ranging between 1.0-1.6Hz. However, it can be pointed that in a frequency range < 1 Hz the response of the primary system is amplified, for values that lie outside the band-gap of the configuration. This phenomenon of beneficial response within frequencies > 1 Hz and amplification for the lower range is intensified for an increasing number of unit cells. Subsequently, in the application of such a structure for vibration mitigation purposes, where an excitation of rich frequency content is applied, there needs to be a balance between the favorable properties of the setup within the band-gap and the unfavorable ones outside of it. To counteract this issue, a factor that can be crucial is the number of unit cells that comprise the metamaterial lattice, where the smaller the number of cells, the lower the amplification outside the band-gap regions.

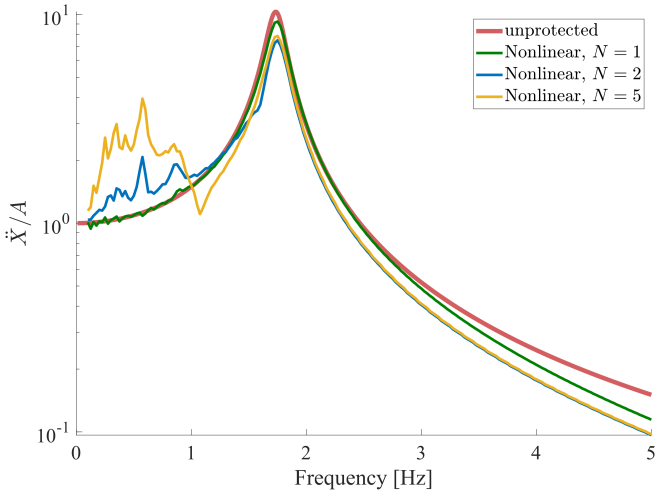

Figure 10: Frequency response function of the absolute acceleration of mass M, protected by the nonlinear configuration (A = 10 m/s2). Comparison to the response of the unprotected structure and an equivalent linear metamaterial.

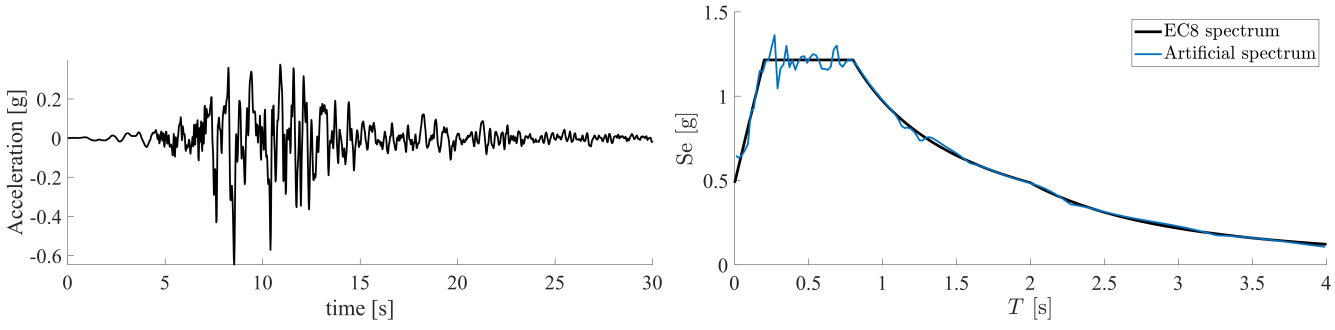

(a) (b)

Figure 11: (a)-Artificial input acceleration time history, (b)-Comparison to the EC8 elastic spectrum (soil type D, a_{gR}=0.36g, γ_i=1).

The effectiveness of the system is further studied on the vibration mitigation potential on the target structure against a realistic input earthquake time history. For this purpose, a modification was performed to the JMA earthquake record [22], so that it meets the elastic spectrum of EC8 [23], according to Ferreira et al. [24], the time history and response spectrum of which are depicted in Figure 11 and is applied to the system of Figure 9 as ground excitation x_g.

Figure 12 displays the acceleration response time history of three individual systems for the earthquake input excitation. The configurations that are studied include the unprotected setup with the consideration of soil-structure interaction, the nonlinear setup of Figure 9 and an equivalent linear system, the two latter consisting of two unit cells each. In the equivalent linear system, the nonlinear element is replaced by a linear relation, the stiffness of which is determined by the tangential stiffness of the triangular arch at the stable equilibrium points. It is observed that both metamaterial configurations are capable of reducing significantly the recorded accelerations at the protected structure, compared to the unprotected case. In terms of the maximum acceleration on the primary mass, the linear system offers a reduction of 16%, while the nonlinear system enhances this reduction to 20%. The effect of the metamaterial design is quantified more clearly by evaluating energy based measures, which can offer additional indication of damage [25]. For this purpose, the calculation of the cumulative total energy (kinetic+potential) of the primary structure is performed as:

$$E_{cum}(t) = \int_0^t E_K(\tau) + E_P(\tau) d\tau \tag{14}$$

where E_K and E_P are the kinetic energy and potential energy respectively.

The comparison of the results depicted in the energy plot of Figure 12 reveals the efficacy of the metamaterial designs. Comparing the nonlinear to the linear application, a further reduction of the total energy is achieved. The linear setup results to a reduction of 29%, compared to the unprotected case, while the nonlinear device improves this reduction to 36%, indicating great potential for further development. It is important to consider that for the investigated setup of Figure 8, the primary structure is strongly connected to the ground via the soil-structure interaction properties. Therefore, any reduction of the output response is seriously more challenging than the case where the protected system is completely detached from the ground. This application can be found useful for retrofitting of existing structures, where the application of vibration mitigation measures below the building is not preferable.

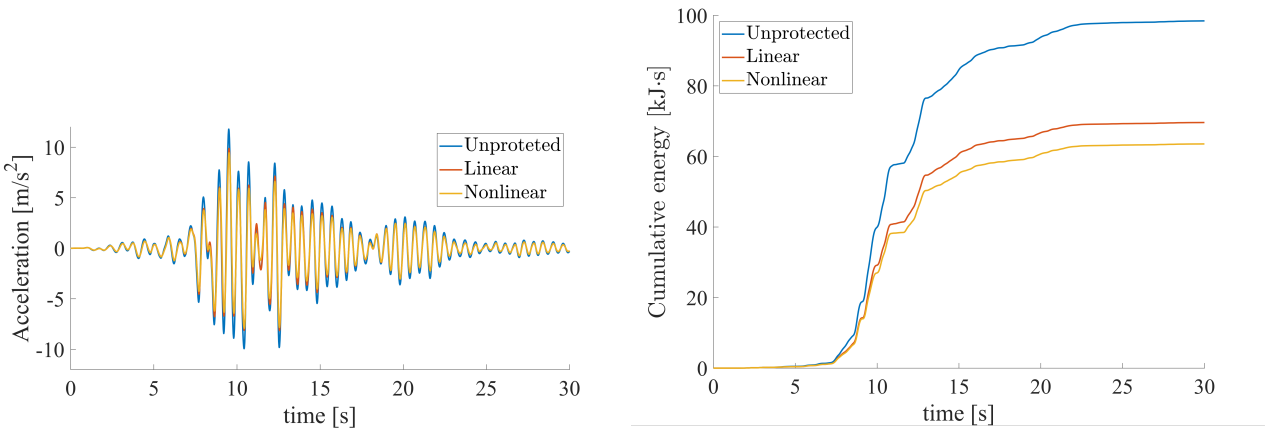

(a) (b)

Figure 12: (a)-Acceleration response of the primary mass. (b)-Cumulative energy of the primary mass. All metamaterial configurations consist of 2 unit cells.

CONCLUSIONS

This study investigates the dynamic properties of a geometrically nonlinear metamaterial device. The dispersion relation of the system is both analytically and numerically investigated. The two approaches are in agreement in terms of the predicted dispersion curves, while the amplitude dependence of the relation has been identified. Therefore, the created band-gap is calculated, indicating the frequency ranges where wave propagation is prohibited. The effectiveness of the configuration is investigated on a reference structure with the consideration of soil-structure interaction. The frequency response of the design is calculated numerically, revealing the beneficial properties that it can offer to the protected structure in terms of vibration mitigation, within the created band-gap. Finally, the response of the protected structure is studied under the application of an earthquake record, which was modified in order to meet the elastic spectrum of EC8, containing the resonance frequency of the protected structure . The results were compared to the conventional unprotected structure and to an equivalent linear system, revealing the significant effect of both the linear and nonlinear metamaterial inclusions, as well as the contribution of nonlinearity in the design. Great potential can be identified for retrofitting purposes of existing structures, where the application of vibration mitigation measures below the foundation of the structure is not possible.

ACKNOWLEDGEMENTS

This project has received funding from the European Union's Horizon 2020 research and innovation programme under the Marie Sklodowska-Curie grant agreement No INSPIRE-813424.

REFERENCES

[1] Z. Zhou, X. Wei, Z. Lu, and B. Jeremic, "Influence of soil-structure interaction on performance of a super tall building using a new eddy-current tuned mass damper," *Struct. Des. Tall Spec. Build.*, vol. 27, no. 14, p. e1501, 2018, doi: 10.1002/tal.1501.

[2] A. F. Vakakis, O. V. Gendelman, L. A. Bergman, D. M. McFarland, G. Kerschen, and Y. S. Lee, *Nonlinear targeted energy transfer in mechanical and structural systems I & II*. Springer Netherlands, 2008.

[3] R. Zaccherini *et al.*, "Locally Resonant Metasurfaces for Shear Waves in Granular Media," *Phys. Rev. Appl.*, vol. 13, p. 034055, 2020, doi: 10.1103/PhysRevApplied.13.034055.

[4] A. Colombi, D. Colquitt, P. Roux, S. Guenneau, and R. V. Craster, "A seismic metamaterial: The resonant metawedge," *Sci. Rep.*, vol. 6, no. 1, p. 27717, 2016, doi: 10.1038/srep27717.

[5] V. K. Dertimanis, I. A. Antoniadis, and E. N. Chatzi, "Feasibility analysis on the attenuation of strong ground motions using finite periodic lattices of mass-in-mass barriers," *J. Eng. Mech.*, vol. 142, no. 9, p. 04016060, 2016, doi: 10.1061/(ASCE)EM.1943-7889.0001120.

[6] V. Fedotov, "Metamaterials," in *Springer Handbooks*, 2017.

[7] F. Bilotti and L. Sevgi, "Metamaterials: Definitions, properties, applications, and FDTD-based modeling and simulation (Invited paper)," *Int. J. RF Microw. Comput. Eng.*, vol. 22, no. 4, pp. 422–438, 2012, doi: 10.1002/mmce.20634.

[8] L. Liu and M. I. Hussein, "Wave motion in periodic flexural beams and characterization of the transition between bragg scattering and local resonance," *J. Appl. Mech. Trans. ASME*, vol. 79, no. 1, p. 011003, 2012, doi: 10.1115/1.4004592.

[9] A. Palermo *et al.*, "Hybridization of Guided Surface Acoustic Modes in Unconsolidated Granular Media by a Resonant Metasurface," *Phys. Rev. Appl.*, vol. 9, no. 5, p. 054026, 2018, doi: 10.1103/PhysRevApplied.9.054026.

[10] R. Zaccherini *et al.*, "Resonant metabarriers as seismic attenuators in granular media," in *Proceedings of ISMA 2018 - International Conference on Noise and Vibration Engineering and USD 2018 - International Conference on Uncertainty in Structural Dynamics*, 2018, pp. 3047–3057.

[11] A. Colombi, R. Zaccherini, G. Aguzzi, A. Palermo, and E. Chatzi, "Mitigation of seismic waves: Metabarriers and metafoundations bench tested," *J. Sound Vib.*, vol. 485, p. 115537, 2020, doi: 10.1016/j.jsv.2020.115537.

[12] M. Wenzel, O. S. Bursi, and I. Antoniadis, “Optimal finite locally resonant metafoundations enhanced with nonlinear negative stiffness elements for seismic protection of large storage tanks,” *J. Sound Vib.*, vol. 483, p. 115488, 2020, doi: 10.1016/j.jsv.2020.115488.

[13] M. H. Bae and J. H. Oh, “Amplitude-induced bandgap: New type of bandgap for nonlinear elastic metamaterials,” *J. Mech. Phys. Solids*, vol. 139, p. 103930, 2020, doi: 10.1016/j.jmps.2020.103930.

[14] C. Daraio, V. F. Nesterenko, E. B. Herbold, and S. Jin, “Tunability of solitary wave properties in one-dimensional strongly nonlinear phononic crystals,” *Phys. Rev. E - Stat. Nonlinear, Soft Matter Phys.*, vol. 73, no. 2, p. 026610, 2006, doi: 10.1103/PhysRevE.73.026610.

[15] K. A. I. Chondrogiannis, V. K. Dertimanis, S. F. Masri, and E. N. Chatzi, “Vibration absorption performance of metamaterial lattices consisting of impact dampers,” in *Proceedings of the International Conference on Structural Dynamic , EURODYN*, 2020, pp. 4139–4149, doi: 10.47964/1120.9338.19599.

[16] P. Martakis, G. Aguzzi, V. K. Dertimanis, E. N. Chatzi, and A. Colombi, “Nonlinear periodic foundations for seismic protection: Practical design, realistic evaluation and stability considerations,” *Soil Dyn. Earthq. Eng.*, vol. 150, p. 106934, 2021, doi: 10.1016/j.soildyn.2021.106934.

[17] Y. Chen, Z. Qian, K. Chen, P. Tan, and S. Tesfamariam, “Seismic performance of a nonlinear energy sink with negative stiffness and sliding friction,” *Struct. Control Heal. Monit.*, vol. 26, no. 11, p. e2437, 2019, doi: 10.1002/stc.2437.

[18] S. Chen *et al.*, “A novel composite negative stiffness structure for recoverable trapping energy,” *Compos. Part A Appl. Sci. Manuf.*, vol. 129, p. 105697, 2020, doi: 10.1016/j.compositesa.2019.105697.

[19] M. A. Al-Shudeifat, “Highly efficient nonlinear energy sink,” *Nonlinear Dyn.*, vol. 76, no. 4, pp. 1905–1920, 2014, doi: 10.1007/s11071-014-1256-x.

[20] D. Alleyne and P. Cawley, “A two-dimensional Fourier transform method for the measurement of propagating multimode signals,” *J. Acoust. Soc. Am.*, vol. 89, no. 3, pp. 1159–1168, 1991, doi: 10.1121/1.400530.

[21] G. Gazetas, “Formulas and charts for impedances of surface and embedded foundations,” *J. Geotech. Eng.*, vol. 117, no. 9, pp. 1363–1381, 1991, doi: 10.1061/(ASCE)0733-9410(1991)117:9(1363).

[22] Pacific Earthquake Engineering Research Center, “PEER Strong Ground Motion Databases,” 2021. https://peer.berkeley.edu/peer-strong-ground-motion-databases.

[23] European Committee for Standardization, “EN 1998-1: Eurocode 8: Design of structures for earthquake resistance – Part 1: General rules, seismic actions and rules for buildings.” 2004.

[24] F. Ferreira, C. Moutinho, Á. Cunha, and E. Caetano, “An artificial accelerogram generator code written in Matlab,” *Eng. Reports*, vol. 2, no. 3, p. e12129, 2020, doi: 10.1002/eng2.12129.

[25] G. Papazafeiropoulos, V. Plevris, and M. Papadrakakis, “A new energy-based structural design optimization concept under seismic actions,” *Front. Built Environ.*, vol. 3, p. 44, 2017, doi: 10.3389/fbuil.2017.00044.